

Multiple scattering effects in Glauber model descriptions of single-nucleon removal reactions

Rui-Ying Chen,¹ Dan-Yang Pang,^{1,2,*} Cen-Xi Yuan,³ Yi-Ping Xu,⁴
Wen-Di Chen,¹ Wen-Long Hai,¹ Jing-Jing Yan,¹ and Wei-Jia Kong¹

¹*School of Physics, Beihang University, Beijing 100191, China*

²*Beijing Key Laboratory of Advanced Nuclear Materials and Physics, Beihang University, Beijing 100191, China*

³*Sino-French Institute of Nuclear Engineering and Technology, Sun Yat-Sen University, Zhuhai 519082, China*

⁴*School of Nuclear Science and Engineering, North China Electric Power University, Beijing 102206, China*

The Glauber/eikonal model is a widely used tool for study of intermediate- and high-energy nuclear reactions. When calculating the Glauber/eikonal model phase-shift functions, the optical limit approximation (OLA) is often used. The OLA neglects the multiple scattering of the constituent nucleons in the projectile and the target nuclei. On the other hand, the nucleon-target version of the Glauber model (the NTG model) proposed by B. Abu-Ibrahim and Y. Suzuki includes multiple scattering effects between the projectile nucleons and the target nuclei. The NTG model has been found to improve the description of the elastic scattering angular distributions and the total reaction cross sections of some light heavy-ion systems with respect to the OLA. In this work, we study the single-nucleon removal reactions (SNRR) induced by carbon isotopes on ¹²C and ⁹Be targets using both the NTG model and the OLA. Reduction factors (RFs) of the single nucleon spectroscopic factors are obtained by comparing the experimental and theoretical SNRR cross sections. It is found that, on average, the RFs obtained with the NTG model is smaller than those using the OLA by 7.8%, in which, the averaged differences in one-neutron removal is 10.6% and those in one-proton removal is 4.2%. But the RFs still have a strong dependence on the neutron-proton asymmetry ΔS of the projectile nuclei even when the NTG model is used.

Keywords: Glauber model of nuclear reactions, single-nucleon removal reactions, spectroscopic factors

I. INTRODUCTION

Measurements and theoretical analysis of single-nucleon removal reactions are of great value for studies of single-particle strengths of atomic nuclei, which are quantitatively represented by spectroscopic factors (SFs) [1]. It is well-known that the SFs extracted from $(e, e'p)$ and single-nucleon transfer reactions are found to be 30% – 50% smaller than those predicted by configuration interaction shell model (CISM) [2, 3]. Such reduction or quenching of SFs, represented by the quenching factors, R_s , is supposed to be originated from the limited model spaces and insufficient treatment of the nucleon-nucleon correlations in the traditional CISM [4, 5]. Unlike the results from $(e, e'p)$ reactions, from single-nucleon transfer reactions [6–8], and from $(p, 2p)$ and (p, pn) reactions [2, 3, 9, 10], where the R_s values of different nuclei are nearly constant, the quenching factors from intermediate energy single-nucleon removal reactions are found to depend almost linearly with the proton-neutron asymmetry of the atomic nuclei, ΔS ($\Delta S = S_p - S_n$ for proton removal and $\Delta S = S_n - S_p$ for neutron removal with S_n and S_p being the neutron and proton separation energies in the ground states of the projectile nuclei, respectively) [11, 12]. For cases when ΔS is larger than around 20 MeV, which correspond to removal of strongly bound nucleons, the R_s values decrease to about 0.3; however, when ΔS is smaller than around -20 MeV, which corresponds to removal of weakly-bound nucleons, the R_s values are close to unity. The reasons why such a clear linear dependence is seen in results of intermediate-energy single-nucleon removal reactions are still not known.

Since most of the single-nucleon removal reactions are analyzed with the Glauber model, validity of the eikonal/Glauber model [11–13] has been put under question [14].

Because of its simplicity, the optical limit approximation (OLA) is often used in the eikonal/Glauber model analysis of the intermediate- and high-energy nuclear reactions [13, 15–19]. Only the first-order term of the expansion of the full Glauber phase shift is taken into account with the OLA. Higher-order interactions, such as the nucleon-nucleon multiple scattering processes are neglected [20]. In Ref. [21], B. Abu-Ibrahim and Y. Suzuki found that although the Glauber model with the OLA can reasonably reproduce the total reaction cross sections of some stable ions on ⁹Be, ¹²C, ²⁷Al targets, it failed to reproduce the reaction cross sections and elastic scattering angular distributions of unstable nuclei. For this, they proposed to calculate the projectile-target phase shifts using nucleon-target interactions in Glauber model calculations. This so-called NTG model (nucleon-target version of the Glauber model) has been found to improve the description of the reaction cross sections and the elastic scattering angular distributions data considerably [21–23]. However, to our knowledge, application of the NTG model to the analysis of single-nucleon knockout reactions and to study its influence on the reduction factors of single particle strengths has not been made yet. In this work, we study how much the R_s values of single-nucleon knockout reactions change when the NTG model is used instead of the usual OLA. Since the NTG model includes multiple scattering effects in the phase-shift functions of the colliding systems with respect to the OLA, we expect this work may give us information about how much the multiple scattering effects will affect the description of single nucleon removal reactions using the Glauber model.

This paper is organized as the following: the NTG model and the OLA of the Glauber model are briefly introduced in

* Corresponding author: dypang@buaa.edu.cn

64 section II; results of our calculations are given in section III,
 65 which include 1) examination of the NTG model about its
 66 reproduction of the elastic scattering and total reaction cross
 67 section data. The cases studied are the angular distributions of
 68 ^{12}C elastic scattering from a carbon target at incident energies
 69 from 30 to 200 MeV/u and the $^{12}\text{C}+^{12}\text{C}$ total reaction cross
 70 sections from 20 to 1000 MeV/nucleon, 2) detailed study of
 71 the NTG model on single-nucleon removal at different in-
 72 cident energies, the case studied here is the $^9\text{Be}(^{19}\text{C}, ^{18}\text{C})\text{X}$
 73 reaction, and 3) effects of the NTG model on the reduc-
 74 tion factors of the single particle strengths. The cases stud-
 75 ied are single nucleon removal cross sections of carbon iso-
 76 topes $^{9,10,12-20}\text{C}$ on ^9Be and carbon targets within 43-250
 77 MeV/nucleon incident energies. The range of ΔS covered in
 78 these reactions is from -26.6 to 20.1 MeV. All results are com-
 79 pared with those of the OLA calculations in order to explicate
 80 the influence of multiple scattering effects in these reactions.
 81 The conclusions are given in section IV.

II. THE NTG MODEL AND THE OLA

83 The NTG model was introduced in Refs. [21, 22]. Details
 84 of its formulae can be found in Ref. [20]. For the convenience
 85 of the readers, we recapitulate the necessary ones here. Let us
 86 start from the phase-shift function of a nucleon-target system,
 87 χ_{NT} , which is defined in the Glauber model framework as
 88 [20]:

$$89 \quad e^{i\chi_{NT}(\mathbf{b})} = \langle \Phi_0^T | \prod_{j=1}^{A_T} [1 - \Gamma_{NN}(\mathbf{b} - \mathbf{t}_j)] \Phi_0^T \rangle, \quad (1)$$

90 where \mathbf{b} is the impact factor vector, \mathbf{t}_j is the projection vector
 91 of the position of the j th nucleon in the target nucleus on the
 92 x - y plane (the beam direction being the z -axis), Γ_{NN} is the
 93 nucleon-nucleon (NN) profile function, which is the Fourier
 94 transform of the NN scattering amplitude, and $|\Phi_0^T\rangle$ is the
 95 wave function of the target nucleus, which has a mass num-
 96 ber A_T . When an independent particle model wave function
 97 is used, which is usually assumed in Glauber model calcula-
 98 tions, the density of the target nucleus can be written as [20]:

$$99 \quad |\Phi_0^T(\mathbf{r}_1, \mathbf{r}_2, \dots, \mathbf{r}_{A_T})|^2 = \prod_{j=1}^{A_T} n_j(\mathbf{r}_j), \quad (2)$$

100 where $n_j(\mathbf{r}_j)$ stands for the normalized density distribution
 101 of the j th nucleon in the target nucleus. The nucleon density
 102 distribution is then

$$103 \quad \rho_T(\mathbf{r}) = \sum_{j=1}^{A_T} n_j(\mathbf{r}). \quad (3)$$

104 With an uncorrelated wave function satisfying Eq. 2, the
 105 nucleon-target phase shift function has the form [20]:

$$106 \quad e^{i\chi_{NT}(\mathbf{b})} = \prod_{j=1}^{A_T} \left[1 - \int d\mathbf{r} n_j(\mathbf{r}) \Gamma_{NN}(\mathbf{b} - \mathbf{t}) \right], \quad (4)$$

107 where \mathbf{t} is the projection of \mathbf{r} on the x - y plane. When the
 108 range of the NN interaction is smaller than the radius of the
 109 target nucleus, which is satisfied in most cases, the integral
 110 $\int d\mathbf{r} n_j(\mathbf{r}) \Gamma_{NN}(\mathbf{b} - \mathbf{t})$ will be smaller than unity [20]. Then
 111 the following approximation could be made [20]:

$$112 \quad 1 - \int d\mathbf{r} n_j(\mathbf{r}) \Gamma_{NN}(\mathbf{b} - \mathbf{t}) \approx e^{- \int d\mathbf{r} n_j(\mathbf{r}) \Gamma_{NN}(\mathbf{b} - \mathbf{t})}. \quad (5)$$

113 One then gets the nucleon-target phase shift of the OLA [20]:

$$114 \quad e^{i\chi_{NT}^{\text{OLA}}(\mathbf{b})} = \prod_{j=1}^{A_T} \exp \left[- \int d\mathbf{r} n_j(\mathbf{r}) \Gamma_{NN}(\mathbf{b} - \mathbf{t}) \right] \\ 115 \quad = \exp \left[- \sum_{j=1}^{A_T} \int d\mathbf{r} n_j(\mathbf{r}) \Gamma_{NN}(\mathbf{b} - \mathbf{t}) \right] \\ 116 \quad = \exp \left[- \int d\mathbf{r} \rho_T(\mathbf{r}) \Gamma_{NN}(\mathbf{b} - \mathbf{t}) \right]. \quad (6)$$

117 This results in the nucleon-nucleus phase-shift function using
 118 the OLA being:

$$119 \quad \chi_{NT}^{\text{OLA}}(\mathbf{b}) = i \int d\mathbf{r} \rho_T(\mathbf{r}) \Gamma_{NN}(\mathbf{b} - \mathbf{t}). \quad (7)$$

120 Note that in Eqs. (1) and (4), multiple scattering terms ap-
 121 pear through cumulant expansions of the phase-shift func-
 122 tions. However, after applying the approximation of Eq. (5)
 123 in Eq. (4), the resulting nucleon-nucleus phase-shift with the
 124 OLA in Eq. (7) contains no multiple scattering terms any-
 125 more [24].

126 Similar to the nucleon-nucleus case in Eq. (1), the nucleus-
 127 nucleus phase shift function, $\chi_{PT}(\mathbf{b})$, for a composite projec-
 128 tile and a target nucleus is [20]:

$$129 \quad e^{i\chi_{PT}(\mathbf{b})} = \langle \Phi_0^P \Phi_0^T | \prod_{i=1}^{A_P} \prod_{j=1}^{A_T} [1 - \Gamma_{NN}(\mathbf{b} + \mathbf{s}_i - \mathbf{t}_j)] \rangle | \Phi_0^P \Phi_0^T \rangle, \quad (8)$$

130 where Φ_0^P is the many-body wave functions of the projectile
 131 (with a mass number A_P) in its ground state. The integrals are
 132 over the coordinates of all the nucleons i and j in the projec-
 133 tile and target nuclei, whose coordinates are \mathbf{r}_i and \mathbf{r}_j , respec-
 134 tively. \mathbf{s}_i and \mathbf{t}_j are their projections on the x - y plane. The
 135 nucleus-nucleus phase shift in this equation contains contri-
 136 butions from single collisions and all order multiple scattering
 137 among the constituent nucleons in the projectile and the target
 138 nuclei. Equation (8) is cumbersome to evaluate directly even
 139 if it is possible. So the optical limit approximation is usually
 140 used and the phase shift function with this approximation is
 141 [20]:

$$142 \quad \chi_{PT}^{\text{OLA}}(\mathbf{b}) = i \int d\mathbf{r}_P \rho_P(\mathbf{r}_P) \int d\mathbf{r}_T \rho_T(\mathbf{r}_T) \Gamma_{NN}(\mathbf{b} + \mathbf{s} - \mathbf{t}), \quad (9)$$

143 where ρ_P and ρ_T are the nucleon density distributions of the
 144 projectile and the target nuclei, respectively, \mathbf{r}_P and \mathbf{r}_T are
 145 the positions of their constituent nucleons, whose projections

146 on the x - y plane are \mathbf{s} and \mathbf{t} respectively. As in the nucleon-
 147 nucleus case in Eq. (7), only single NN collisions contribute
 148 to this phase shift. Contributions from multiple scatterings
 149 are missing, which could be, to some extent, recovered by
 150 the nucleon-target version of the Glauber model (the NTG
 151 model) proposed by Abu-Ibrahim and Suzuki [20–23].

152 The idea of the NTG model is to replace $\langle \Phi_0^T | \prod_{j \in T} [1 -$
 153 $\Gamma_{NN}(\mathbf{b} + \mathbf{s}_i - \mathbf{t}_j)] | \Phi_0^T \rangle$ for each nucleon i in the projectile in
 154 Eq. (8) by

$$155 \quad \langle \Phi_0^T | \prod_{j=1}^{A_T} [1 - \Gamma_{NN}(\mathbf{b} + \mathbf{s}_i - \mathbf{t}_j)] | \Phi_0^T \rangle \\ 156 \quad \equiv 1 - \Gamma_{NT}(\mathbf{b} + \mathbf{s}_i), \quad (10)$$

157 where $\Gamma_{NT}(\mathbf{b} + \mathbf{s}_i)$ is the profile function of its collision
 158 with the target nucleus. The nucleus-nucleus phase shift then
 159 takes the form [20]:

$$160 \quad e^{i\chi_{PT}^{\text{NTG}}(\mathbf{b})} = \langle \Phi_0^P | \prod_{i=1}^{A_P} [1 - \Gamma_{NT}(\mathbf{b} + \mathbf{s}_i)] | \Phi_0^P \rangle. \quad (11)$$

161 This is the so-called NTG model. Following the same proce-
 162 dure of obtaining the Eq. (7), the phase shift of the projectile-
 163 target system with the NTG model is:

$$164 \quad \chi_{PT}^{\text{NTG}}(\mathbf{b}) = i \int d\mathbf{r} \rho_P(\mathbf{r}) \Gamma_{NT}(\mathbf{b} + \mathbf{s}), \quad (12)$$

165 and the nucleon-target profile function, Γ_{NT} is:

$$166 \quad \Gamma_{NT}(\mathbf{b} + \mathbf{s}_i) \\ 167 \quad = 1 - \langle \Phi_0^T | \prod_{j=1}^{A_T} [1 - \Gamma_{NN}(\mathbf{b} + \mathbf{s}_i - \mathbf{t}_j)] | \Phi_0^T \rangle \\ 168 \quad = 1 - \exp \left[- \int d\mathbf{r}_T \rho_T(\mathbf{r}_T) \Gamma_{NN}(\mathbf{b} + \mathbf{s} - \mathbf{t}) \right]. \quad (13)$$

169 Substituting this Γ_{NT} in Eq. (12), we get the nucleus-nucleus
 170 phase shift function of the NTG model:

$$171 \quad \chi_{PT}^{\text{NTG}}(\mathbf{b}) = i \int d\mathbf{r}_P \rho_P(\mathbf{r}_P) \\ 172 \quad \times \left\{ 1 - \exp \left[- \int d\mathbf{r}_T \rho_T(\mathbf{r}_T) \Gamma_{NN}(\mathbf{b} + \mathbf{s} - \mathbf{t}) \right] \right\} \quad (14)$$

173 That the nucleus-nucleus phase shift of the NTG model
 174 contains multiple scattering effects other than the OLA can be
 175 seen by power expansion of the nucleon-target profile func-
 176 tion of Eq. (13):

$$177 \quad \Gamma_{NT}(\mathbf{b} + \mathbf{s}_i) \\ 178 \quad = \int d\mathbf{r}_T \rho_T(\mathbf{r}_T) \Gamma_{NN}(\mathbf{b} + \mathbf{s} - \mathbf{t}) - \\ 179 \quad \frac{1}{2!} \left[\int d\mathbf{r}_T \rho_T(\mathbf{r}_T) \Gamma_{NN}(\mathbf{b} + \mathbf{s} - \mathbf{t}) \right]^2 + \dots \quad (15)$$

180 The first term is contributed by single scattering of the pro-
 181 jectile nucleon from nucleons in the target nucleus. The sec-
 182 ond and other terms represent contributions from multiple NN

183 scattering [20]. Clearly, if only the first term is used in Eq.
 184 (12), the NTG phases shift will reduce to that of the OLA in
 185 Eq. (9). By taking into account the higher order terms in Eq.
 186 (15), phase shifts with the NTG model recover some multiple
 187 scattering effects that are missing with the OLA. One should
 188 note, however, that the contributions from multiple scattering
 189 processes included in this way is not identical to those in full
 190 Glauber model in Eqs. (1) and (8) [25]. Nevertheless, as we
 191 will show in the next section, the NTG model could improve
 192 the description of the elastic scattering angular distributions,
 193 especially at low incident energies, and total reaction cross
 194 sections for the $^{12}\text{C} + ^{12}\text{C}$ test case within a rather wide range
 195 of incident energies. Practically, a symmetrized version of the
 196 NTG phase shift is often calculated [21, 23]:

$$197 \quad \chi_{PT}^{\text{NTG}}(\mathbf{b}) = \frac{i}{2} \int d\mathbf{r}_P \rho_P(\mathbf{r}_P) \left\{ 1 - \right. \\ 198 \quad \left. \exp \left[- \int d\mathbf{r}_T \rho_T(\mathbf{r}_T) \Gamma_{NN}(\mathbf{b} + \mathbf{s} - \mathbf{t}) \right] \right\} \\ 199 \quad + \frac{i}{2} \int d\mathbf{r}_T \rho_T(\mathbf{r}_T) \left\{ 1 - \right. \\ 200 \quad \left. \exp \left[- \int d\mathbf{r}_P \rho_P(\mathbf{r}_P) \Gamma_{NN}(\mathbf{b} + \mathbf{t} - \mathbf{s}) \right] \right\}. \quad (16)$$

201 202 However, the phase-shifts calculated with Eqs. (14) and (16)
 203 are often very close to each other [21, 22].

204 205 The profile function Γ_{NN} in the both the OLA and the
 206 NTG model calculations is parameterized in a Gaussian form:

$$206 \quad \Gamma_{pN}(\mathbf{b}) = \frac{1 - i\alpha_{pN}}{4\pi\beta_{pN}} \sigma_{pN}^{\text{tot}} \exp \left(-\frac{\mathbf{b}^2}{2\beta_{pN}} \right), \quad (17)$$

207 208 where the Γ_{NN} parameters σ_{pN}^{tot} , α_{pN} , and β_{pN} are the
 209 210 proton-nucleon total cross section, the ratio of the real to
 211 212 imaginary part of the p - N scattering amplitudes, and the cor-
 213 214 responding slope parameter [26], respectively. Due to the
 215 216 lack of experimental data on neutron-neutron scattering, Γ_{pp}
 217 218 is commonly used instead of Γ_{NN} . In this work, σ_{pN}^{tot} are
 219 220 taken from Ref. [27], which is parameterized by fitting the ex-
 221 222 perimental data from Ref. [28], the α_{pN} parameters are taken
 223 224 from those tabulated from Ref. [26] for a range of incident en-
 225 226 ergies from 100 to 2200 MeV/u. If the beam energy is lower
 227 228 than 100 MeV/u, we take the value corresponding to lowest
 229 230 energy from the table. The finite range slope parameters β_{pN}
 231 232 are taken to be 0.125 fm², in accordance with systematic stud-
 233 234 ies of single-nucleon removal reaction [13, 15, 29].

221 III. COMPARISONS BETWEEN THE NTG MODEL AND 222 OLA IN GLAUBER MODEL CALCULATIONS

223 224 In Ref. [30], T. Nagashisa and W. Horiuchi demonstrated
 225 226 the effectiveness of the NTG by comparing the description
 227 228 of the total reaction cross sections using the full Glauber
 229 230 model calculation, the NTG model, and the OLA for cases
 231 232 of $^{12,20,22}\text{C}$ on a ^{12}C target at various incident energies. In
 233 234 this work, our main purpose is to study how much the single-
 235 236 nucleon removal cross sections (σ_{-1N}) will change when the

230 NTG model instead of the OLA is used. Before calculating
 231 σ_{-1N} , we need to firstly compare our calculations for the
 232 elastic scattering angular distributions and total reaction cross
 233 sections with experimental data and with the predictions of
 234 the OLA. The calculations are made for the $^{12}\text{C}+^{12}\text{C}$ system.
 235 By doing so, we also verify the effectiveness of the Γ_{NN} pa-
 236 rameters used in our calculations, which are further used in
 237 the calculations of σ_{-1N} . The single-nucleon removal reac-
 238 tions are calculated using a modified version of the computer
 239 code MOMDIS [31].

240 A. Elastic scattering angular distributions and total reaction 241 cross sections

242 The angular distributions of ^{12}C elastic scattering from a
 243 ^{12}C target at 30, 85, 120, and 200 MeV/nucleon are calcu-
 244 lated with both the OLA and the NTG model. The results are
 245 shown in Fig. 1 together with the experimental data. Clearly,
 246 the NTG improved the description of the $^{12}\text{C}+^{12}\text{C}$ elastic
 247 scattering considerably with respect to the OLA, especially
 248 when the incident energy is below around 100 MeV/nucleon.
 249 This can be expected because the multiple scattering effect,
 250 which are included in the NTG model but not in the OLA,
 251 should be more important at low incident energies than at
 252 higher incident energies. Note that other corrections due to,
 253 for instance, the antisymmetrization of the projectile and tar-
 254 get wavefunctions [32], the Fermi motion of the nucleons in
 255 the colliding nuclei [33], distortion of the trajectories [18],
 256 can also affect the low-energy cross sections. More complete
 257 calculations taking these aspect together might be an interest-
 258 ing subject for future.

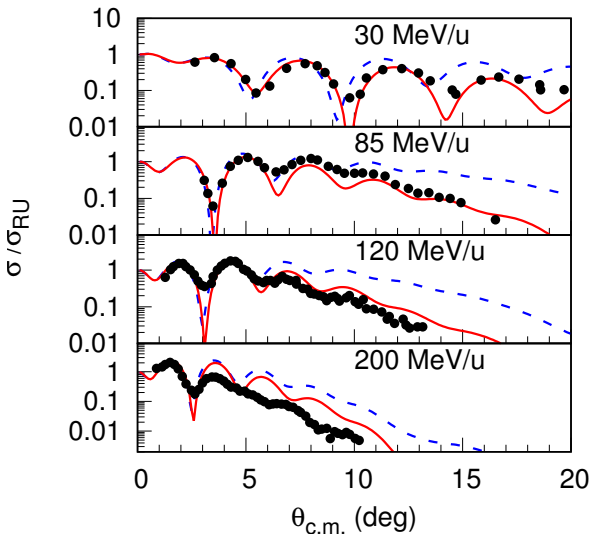


Fig. 1. Elastic scattering angular distributions of ^{12}C on a carbon target at incident energies of 30, 85, 120, and 200 MeV/nucleon. The red solid and blue dashed curves are results of Glauber model calculations with the NTG model and the OLA, respectively. The dots are experimental data from Refs. [34, 35].

259 Comparison between the NTG and OLA predictions to the

260 total reaction cross sections of the $^{12}\text{C}+^{12}\text{C}$ system is shown
 261 in Fig. 2. Again, we see that results of the NTG model have
 262 better agreement with the experiment data than those of the
 263 OLA, especially for the incident energies at several tens of
 264 MeV/nucleon and above, where most of the one-nucleon re-
 265 moval cross section data were measured [12]. In both elas-
 266 tic scattering and total reaction cross section calculations, the
 267 proton and neutron density distributions of the ^{12}C nucleus
 268 are taken to be a Gaussian form with a root-mean-square ra-
 269 dius of 2.32 fm [12], which is very close to the 2.33 ± 0.01
 270 fm from elastic electron scattering data [36].

271 Note that the Γ_{NN} parameters are the same in both NTG
 272 and OLA calculations. The only difference between these
 273 two methods is that the former introduced multiple scattering
 274 effects in the calculation of eikonal phase functions. The im-
 275 provement provided by the NTG model in the description of
 276 elastic scattering angular distributions and the total reaction
 277 cross sections suggests that nuclear medium effects, such as
 278 the multiple scattering effect studied here, should be taken
 279 into account in Glauber model description of the nuclear re-
 280 actions induced by heavy-ions. In the following section, we
 281 study how the NTG model could affect the theoretical pre-
 282 dictions of the single-neutron removal cross sections and the
 283 single particle strengths obtained from the experimental data.

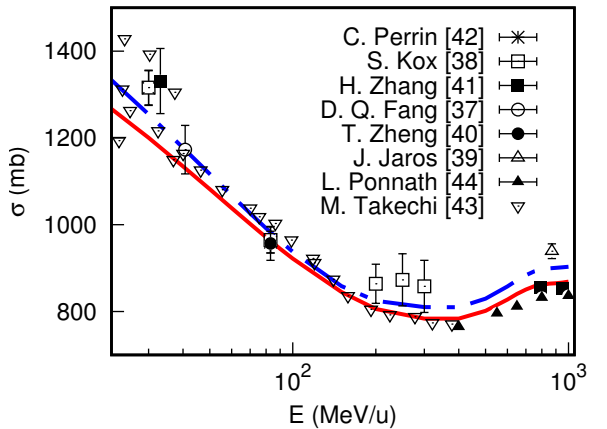


Fig. 2. Reaction cross sections of ^{12}C on a carbon target. The red solid and blue dash-dotted curves are results of Glauber model cal-
 culations with the NTG model and the OLA, respectively. The symbols represent experimental data from Ref. [37–44].

284 B. Single-nucleon removal cross sections at different incident 285 energies

286 In an inclusive single-nucleon removal reaction, $A(a, b)X$,
 287 where only the core nucleus b ($A_b = A_a - 1$) is detected, two
 288 processes may happen: the diffraction dissociation and strip-
 289 ping, which correspond to the valence neutron escaped or be-
 290 ing captured by the target nucleus, respectively. Within the
 291 Glauber model framework, their cross sections, σ_{sp}^{dd} and σ_{sp}^{str} ,

292 respectively, are calculated by: [45]:

$$293 \quad \sigma_{sp}^{dd} = \frac{1}{2j+1} \sum_m \int d\mathbf{b} \left[\left\langle \psi_{nljm} \left| \left(1 - S_v S_c\right)^2 \right| \psi_{nljm} \right\rangle \right. \\ 294 \quad \left. - \sum_{m'} \left| \left\langle \psi_{nljm'} \left| \left(1 - S_v S_c\right) \right| \psi_{nljm} \right\rangle \right|^2 \right], \quad (18)$$

295 and

$$296 \quad \sigma_{sp}^{str} = \frac{1}{2j+1} \sum_m \int d\mathbf{b} |S_c|^2 \times \\ 297 \quad \left\langle \psi_{nljm} \left| \left(1 - |S_v|^2\right) \right| \psi_{nljm} \right\rangle. \quad (19)$$

298 Here $S_c = e^{i\chi_{cT}}$ and $S_v = e^{i\chi_{vT}}$ are the core-target and
299 the valence nucleon-target S -matrices, respectively. The va-
300 lence nucleon-target phase shift function χ_{vT} is calculated
301 with Eq. (7), and the core-target phase shift function χ_{cT} is
302 calculated according to Eq. (9) for the OLA and Eq. (16) for
303 the NTG model; \mathbf{b} is the impact factor vector of the projec-
304 tile in the plane perpendicular to the beam direction, ψ_{nljm} is
305 the single-particle wave function (SPWF) with n , l , and j be-
306 ing the principal, the angular momentum, and the total angular
307 momentum numbers respectively, and m is the projection
308 of j . Equations (7, 9, 14 and 16) are about nuclear phase-
309 shift only. For charged particles, one also has to include the
310 Coulomb phase-shift [31]:

$$311 \quad \chi_C = 2\eta \ln(kb), \quad (20)$$

312 where $\eta = Z_1 Z_2 e^2 \mu / \hbar^2 k$ is the Sommerfeld parameter with
313 Z_1 and Z_2 being the charge numbers of the two colliding par-
314 ticles, whose reduced mass is μ , and k being the wave num-
315 ber in the center of mass system. The single-particle wave
316 functions are associated with the specific states of the core
317 with spin I_b and the composite nuclei with spin I_a by spec-
318 troscopic factors, $(C^2 S)_{I_a I_b, nlj}$. So, the single-particle cross
319 section of removal of a nucleon from the ground state of a
320 projectile leaving the core nucleus in a specific state with the
321 SPWF having quantum numbers nlj is:

$$322 \quad \sigma_{sp}(I_a I_b, nlj) = \left(\frac{A}{A-1} \right)^N (C^2 S)_{I_a I_b, nlj} \times (\sigma_{sp}^{dd} + \sigma_{sp}^{str}), \quad (21)$$

323 where the $[A/(A-1)]^N$ factor is for the center-of-mass cor-
324 rections to the spectroscopic factor $C^2 S$ [46], and $N = 2n+l$
325 is the number of oscillator quanta associated with the major
326 shell of the removed particle (the minimum value of n is taken
327 to be zero).

328 Experimentally, single-nucleon removal cross sections are
329 usually measured inclusively, namely, only the core nucleus
330 b is measured without discriminating its energy states. Cor-
331 respondingly, theoretical calculations for these measurements
332 should also include the contributions from all the bound ex-
333 cited states of the core nucleus b [13], which corresponds to
334 summation of all the single-particle cross sections associated
335 with all possible single particle wave functions:

$$336 \quad \sigma_{-1N}^{\text{th}} = \sum_{nlj, I_b} \sigma_{sp}(I_a I_b, nlj). \quad (22)$$

TABLE 1. Single neutron removal cross sections of ^{19}C on a beryllium target at incident energies of 64, 100, 200, and 400 MeV/nucleon calculated with the NTG model, $\sigma_{-1n}^{\text{NTG}}$, and the OLA, $\sigma_{-1n}^{\text{OLA}}$. The state of the core nucleus and their corresponding single-nucleon spectroscopic factors are taken from Ref. [15].

E_{inc}	E_x	J^π	nlj	$C^2 S$	$\sigma_{-1n}^{\text{OLA}}$	$\sigma_{-1n}^{\text{NTG}}$	$\sigma_{-1n}^{\text{NTG}}/\sigma_{-1n}^{\text{OLA}}$
64	0.000	0^+	$1s_{1/2}$	0.580	104.31	109.3	1.050
	2.144	2^+	$0d_{5/2}$	0.470	18.93	21.16	1.118
	3.639	2^+	$0d_{5/2}$	0.104	3.53	3.98	1.127
	3.988	0^+	$1s_{1/2}$	0.319	17.82	19.72	1.107
	4.915	3^+	$0d_{5/2}$	1.523	46.18	52.21	1.131
	4.975	2^+	$0d_{5/2}$	0.922	27.83	31.46	1.130
	Inclusive				218.42	237.83	1.089
100	0.000	0^+	$1s_{1/2}$	0.580	87.58	90.14	1.029
	2.144	2^+	$0d_{5/2}$	0.470	17.95	19.13	1.066
	3.639	2^+	$0d_{5/2}$	0.104	3.41	3.64	1.067
	3.988	0^+	$1s_{1/2}$	0.319	16.43	17.44	1.061
	4.915	3^+	$0d_{5/2}$	1.523	45.05	48.24	1.071
	4.975	2^+	$0d_{5/2}$	0.922	27.15	29.08	1.071
	Inclusive				197.57	207.67	1.051
200	0.000	0^+	$1s_{1/2}$	0.580	61.66	63.55	1.031
	2.144	2^+	$0d_{5/2}$	0.470	15.46	16.52	1.069
	3.639	2^+	$0d_{5/2}$	0.104	3.01	3.23	1.073
	3.988	0^+	$1s_{1/2}$	0.319	13.47	14.30	1.062
	4.915	3^+	$0d_{5/2}$	1.523	40.59	43.61	1.071
	4.975	2^+	$0d_{5/2}$	0.922	24.48	26.31	1.075
	Inclusive				158.67	167.52	1.056
400	0.000	0^+	$1s_{1/2}$	0.580	54.76	57.04	1.042
	2.144	2^+	$0d_{5/2}$	0.470	14.61	16.00	1.095
	3.639	2^+	$0d_{5/2}$	0.104	2.87	3.16	1.101
	3.988	0^+	$1s_{1/2}$	0.319	12.54	13.57	1.082
	4.915	3^+	$0d_{5/2}$	1.523	38.80	42.91	1.106
	4.975	2^+	$0d_{5/2}$	0.922	23.41	25.89	1.106
	Inclusive				146.99	158.57	1.079

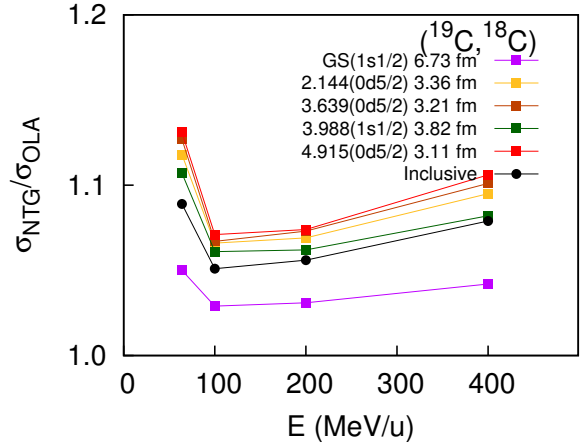


Fig. 3. Ratios of the NTG and OLA predicted single particle cross sections associated with different core states of the $^9\text{Be}(^{19}\text{C}, ^{18}\text{C})$ reaction at incident energies 64, 100, 200, and 400 MeV/nucleon. The excitation energies of the core nucleus ^{18}C and the properties of their corresponding single-particle wave functions – their nlj values and root-mean-square radii – are also shown. The lines are to guide eyes.

337 In order to see how much difference the NTG model pre-
 338 dicts the single-nucleon removal cross sections with respect
 339 to the OLA, we study the $(^{19}\text{C}, ^{18}\text{C})$ reaction on a ^9Be tar-
 340 get at 64, 100, 200, and 400 MeV/nucleon incident energies.
 341 The excited states of the ^{18}C nucleus, the associated single
 342 particle wave functions, and their corresponding shell model
 343 predicted spectroscopic factors are taken to be the same as
 344 those in Ref. [15]. The single particle wave functions are cal-
 345 culated with single particle potentials of Woods-Saxon forms
 346 with the depths adjusted to provide the experimental separa-
 347 tion energies of the valence nucleon, and the radius and dif-
 348 fuseness parameters are taken to be $r_0 = 1.25$ fm and $a = 0.7$
 349 fm, respectively, the same as those used in Ref. [15]. The re-
 350 sults are shown in Table. 1. Single-nucleon removal cross
 351 sections with the NTG model and the OLA are denoted as
 352 $\sigma_{-1n}^{\text{NTG}}$ and $\sigma_{-1n}^{\text{OLA}}$, respectively. Note that the $\sigma_{-1n}^{\text{OLA}}$ values at
 353 64 MeV/nucleon agree very well with those reported in Ref.
 354 [15]. The ratios between $\sigma_{-1n}^{\text{NTG}}$ and $\sigma_{-1n}^{\text{OLA}}$, are also depicted in
 355 Fig. 3.

356 It is interesting to observe that:

- 357 1. the one-nucleon removal cross sections calculated
 358 with the NTG model is larger than those with the
 359 OLA within the whole energy range from 50 to 400
 360 MeV/nucleon,
- 361 2. Such differences are larger at incident energies
 362 smaller than around 100 MeV/nucleon, almost constant
 363 around 100-200 MeV/nucleon, and increase slightly
 364 when the incident energy is larger than around 200
 365 MeV/nucleon,
- 366 3. The differences are also bigger when the root-mean-
 367 square radius of the single particle wave function is
 368 smaller, which means that the NTG model is especially
 369 important for one-neutron removal cross sections of a
 370 given reaction when the single nucleon is tightly bound.

371 The same are found for other nuclei studied in this work.
 372 The difference between the NTG model and the OLA is in
 373 the core-target S -matrix, S_c , only. However, as we see from
 374 Eqs. (18) and (19), we are not able to separate S_c from S_v
 375 and the single particle wave functions in the calculation of
 376 single-nucleon removal cross sections. Thus, we can not ex-
 377 hibit the details how the NTG model along affects the σ_{-1n}
 378 values with respect to the OLA. In the following subsection,
 379 we study how the spectroscopic factors extracted from the ex-
 380 perimental data and their reduction factors change when the
 381 NTG model instead of the OLA is used.

382 C. Reduction factors of single particle strengths

The spectroscopic factors in Eq. (22) are often taken from configuration interaction shell model (CISM) calculations in calculating the one-nucleon removal cross sections. Due to limited model spaces and insufficient treatment of nucleon-nucleon correlations, It is well-known that the CISM predicted SFs are usually larger than the experimental ones. Reduction factors of the SFs, R_s , which are ratios between

the experimental and theoretical SFs, are defined to quantify such differences. For the case of inclusive single-nucleon knockout reactions, the reduction factors are defined as the ratios between the experimental and theoretical cross sections [11, 12]:

$$383 R_s = \sigma_{-1N}^{\text{exp}} / \sigma_{-1N}^{\text{th}}.$$

384 For nuclei that have more than one sets of experimental data
 385 available, a weighted mean of the R_s values for each mea-
 386 surement is used [47]:

$$386 \mathfrak{R} = \frac{\sum_i R_{si} w_i}{\sum_i w_i}, \quad (23)$$

387 where the weights are defined by the errors of the individual
 388 R_s values (ΔR_{si}):

$$389 w_i = \left[\frac{1}{\Delta R_{si}} \right]^2,$$

390 and the errors of the averaged \mathfrak{R} is:

$$391 \Delta \mathfrak{R} = \frac{1}{\sqrt{\sum_i w_i}}.$$

392 The effective neutron-proton asymmetry ΔS_{eff} is given
 393 by[[15]]

$$394 \Delta S_{\text{eff}} = S_n + \bar{E}_f - S_p, \text{ for neutron removal,}$$

$$395 \Delta S_{\text{eff}} = S_p + \bar{E}_f - S_n, \text{ for proton removal,}$$

396 where \bar{E}_f is obtain by weighting the excitation energy E^* of
 397 each final state by the single nucleon removal cross section to
 398 that state.

399 Using the method described in the previous subsection, we
 400 analyzed a series of single-nucleon removal reaction data.
 401 Details of these reactions, such as the target nuclei used, the
 402 incident energies are given in Table. 2. The theoretical pre-
 403 dicted single-nucleon removal cross sections using the NTG
 404 and the OLA, $\sigma_{-1N}^{\text{NTG}}$ and $\sigma_{-1N}^{\text{OLA}}$, respectively, are also listed
 405 together with the experimental single-nucleon removal cross
 406 sections, $\sigma_{-1N}^{\text{exp}}$, and the reduction factors, $\mathfrak{R}^{\text{NTG}}$ and $\mathfrak{R}^{\text{OLA}}$,
 407 respectively. The single-particle spectroscopic factors ($C^2 S$)
 408 used in these calculations are taken from references corre-
 409 sponding to the experimental data and Refs. [47]. These re-
 410 duction factors are depicted in Fig. 4 as functions of neutron-
 411 proton asymmetry. Since many σ_{-1N} were measured in-
 412 clusively, namely, they include all bound states of the core
 413 nuclei, which correspond to different separation energies of
 414 the removed nucleon, an effective neutron-proton asymme-
 415 try is used here: $\Delta S_{\text{eff}} = S_n + \bar{E}_f - S_p$ for neutron re-
 416 moval and $\Delta S_{\text{eff}} = S_p + \bar{E}_f - S_n$ for proton removal, where
 417 \bar{E}_f is the weighted mean excitation energy of the core nu-
 418 cleus, $\bar{E}_f = (\sum_i E_{\text{ex},i} \sigma_{sp,i}) / \sum_i \sigma_{sp,i}$, with $E_{\text{ex},i}$ and $\sigma_{sp,i}$
 419 being the excitation energy of the core nucleus in its i -th
 420 state and the corresponding single particle cross section with
 421 Eq. (21) [11]. In all these calculations, the single particle
 422 wave functions are calculated with Woods-Saxon potentials

whose radius parameters, r_0 , are determined with the HF calculations [48] and the diffuseness parameters being fixed as $a = 0.65$ fm except for the $^{15,17,18}\text{C}$ projectiles, for which, the $r_0 = 1.15$ fm and $a = 0.50$ fm is used following Ref. [49]. And for proton removal of ^{16}C , $r_0 = 1.40$ fm and $a = 0.70$ fm is used following Ref. [50]. The proton and neutron density distributions of the nucleus ^9Be are taken to be a Gaussian form with a root-mean-square radius of 2.36 fm [12].

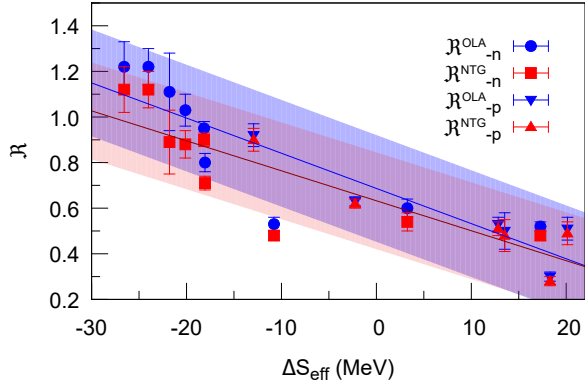


Fig. 4. Averaged reduction factors \mathfrak{R} listed in Table. 2 as functions of the effective neutron-proton asymmetry ΔS_{eff} . The red squares and blue dots are results of the neutron removal of the NTG model and the OLA, respectively. The red triangles and blue inverted triangles are the same but for proton removal. The light red and blue bands represent the widths of their distributions.

As one can see from Table. 2, σ_{-1N} values predicted with the NTG model are generally larger than those with the OLA. Thus, the \mathfrak{R} values with the NTG are smaller than those with the OLA. On average, the changes in the \mathfrak{R} values induced by the NTG model with respect to the OLA are about 7.8%. However, as one can see from Fig. 4, that the \mathfrak{R} values with the NTG model and the OLA, $\mathfrak{R}^{\text{NTG}}$ and $\mathfrak{R}^{\text{OLA}}$, respectively, still depend linearly on the effective neutron-proton asymmetry ΔS_{eff} , although the slope with the NTG model is 18% smaller than that with the OLA. The parameters of this linear dependence are:

$$\begin{aligned} \mathfrak{R}^{\text{OLA}} &= 0.687 - 0.0154\Delta S_{\text{eff}}, \\ \mathfrak{R}^{\text{NTG}} &= 0.633 - 0.0131\Delta S_{\text{eff}}. \end{aligned} \quad (24)$$

So the systematics of the \mathfrak{R} values with respect to ΔS_{eff} observed in Refs. [11, 12] persist even when the multiple scattering effects inherited in the NTG model are included in the Glauber model calculations.

Looking more closely at Fig. (4), one sees that the differences between $\mathfrak{R}^{\text{NTG}}$ and $\mathfrak{R}^{\text{OLA}}$ in the most negative ΔS_{eff} region are larger than at the most positive ΔS_{eff} region. To be more specific, the averaged differences between $\mathfrak{R}^{\text{NTG}}$ and $\mathfrak{R}^{\text{OLA}}$ is 9.9% for $\Delta S_{\text{eff}} < -10$ MeV and 5.3% for $\Delta S_{\text{eff}} > 10$ MeV. This seems to suggest that the multiple scattering effect introduced with the NTG model is more important for removal of weakly bound nucleons than for deeply bound ones. This is misleading. It happens that most of the

cases in the $\Delta S_{\text{eff}} < -10$ MeV region are single neutron removal reactions, and those in the $\Delta S_{\text{eff}} > 10$ MeV region are single proton removal reactions. From the $\mathfrak{R}^{\text{NTG}}$ and $\mathfrak{R}^{\text{OLA}}$ values shown in Table. 2, one sees that the average differences between $\mathfrak{R}^{\text{NTG}}$ and $\mathfrak{R}^{\text{OLA}}$ are 10.6% and 4.2% for neutron and proton removal reactions, respectively. Currently, it is not clear why the effect of the NTG model has such systematic differences to these two types of reactions. As we discussed at the end of the last section, the only difference between the NTG model and the OLA is in the core-target S -matrices, S_c . However, as one sees from Eqs. (18) and (19), S_c can not be singled out from S_v and the single-particle wave functions when calculating the single-nucleon removal cross sections. This means that the multiple scattering effects induced in the NTG model to σ_{-1N} through S_c are moderated by the single particle wave functions, which are different for different cases. So we are not able to explicitly show how the NTG model alone affects the σ_{-1N} values and why it behaves differently for proton and neutron removal reactions.

IV. SUMMARY

The reduction of the single-particle strengths, represented by the reduction factors of single-nucleon spectroscopic factors extracted from experimental data with respect to configuration interaction shell model predictions, is supposed to be related to the nucleon-nucleon correlations in atomic nuclei. Quite a lot of theoretical and experimental efforts have been devoted to this area. One of the open questions is why the reduction factors obtained from intermediate- and high-energy single nucleon removal cross sections as those compiled in Refs. [11, 12] show strong linear dependence on the neutron-proton asymmetry, whereas those of other types of reactions, such as (p,pN) and single nucleon transfer reactions do not [2, 3, 6, 9, 64, 65]. Since the single-nucleon removal reactions were analyzed with the Glauber model, validity of the Glauber model on such reactions is being questioned. With this respect, corrections to the Glauber model and examination of their effects on the single-nucleon removal cross sections become important.

In this work, we examine how the nucleon-target version of the Glauber model (the NTG model), which introduces multiple scattering of the constituent nucleons in the projectile and the target nuclei, could change the theoretical predicted single-nucleon removal cross sections with respect to the usual optical limit approximation, which does not contain multiple scattering effects. For this purpose, we firstly examined the NTG model in its reproduction of the elastic scattering angular distributions and the total reaction cross sections of the $^{12}\text{C}+^{12}\text{C}$ system, and compare their results with the experimental data and those calculated with the OLA. The NTG model is found to improve the description of the elastic scattering angular distributions, especially at lower incident energies. Both the elastic scattering and total reaction cross sections calculated in this work agree well with those reported in previous publications, e.g., Refs. [21, 23, 30].

We then compare the predictions of inclusive single-

TABLE 2. Experimental ($\sigma_{-1N}^{\text{exp}}$) and theoretical inclusive single-nucleon removal cross sections calculated with the OLA ($\sigma_{-1N}^{\text{OLA}}$) and the NTG model ($\sigma_{-1N}^{\text{NTG}}$), and the corresponding reductions factors $\mathfrak{R}^{\text{OLA}}$ and $\mathfrak{R}^{\text{NTG}}$.

Reaction	ΔS_{eff}	Target	E_{inc}	$\sigma_{-1N}^{\text{exp}}$	$\sigma_{-1N}^{\text{OLA}}$	$\sigma_{-1N}^{\text{NTG}}$	$\mathfrak{R}^{\text{OLA}}$	$\mathfrak{R}^{\text{NTG}}$
($^{20}\text{C}, ^{19}\text{C}$)	-26.574	C	240	58(5) [51]	47.55	51.88	1.22(11)	1.12(10)
($^{19}\text{C}, ^{18}\text{C}$)	-24.142	Be	57	264(80) [52]	179.06	201.62	1.47(45)	1.31(40)
	-24.104	Be	64	226(65) [53]	176.69	195.48	1.28(37)	1.16(33)
	-23.754	C	243	163(12) [51]	134.75	146.63	1.21(9)	1.11(8)
Average	-24.022						1.22(8)	1.12(8)
($^{18}\text{C}, ^{17}\text{C}$)	-21.793	C	43	115(18) [49]	103.20	128.70	1.11(17)	0.89(14)
($^{17}\text{C}, ^{16}\text{C}$)	-20.130	C	49	84(8) [49]	92.80	109.70	0.91(9)	0.77(7)
	-20.121	Be	62	115(14) [52]	87.80	100.77	1.31(16)	1.14(14)
	-20.121	Be	79	116(18) [54]	90.37	100.48	1.28(20)	1.15(18)
Average	-20.124						1.03(7)	0.88(6)
($^{15}\text{C}, ^{14}\text{C}$)	-18.275	C	54	137(16) [49]	180.56	196.44	0.76(9)	0.70(8)
	-18.242	C	62	159(15) [49]	176.11	189.78	0.90(8)	0.84(8)
	-18.169	C	83	146(23) [37]	166.44	176.08	0.88(14)	0.83(13)
	-17.879	Be	103	146(23) [53]	142.52	149.89	0.98(3)	0.94(3)
Average	-18.155						0.95(3)	0.90(0)
($^{16}\text{C}, ^{15}\text{C}$)	-18.055	C	55	65(6) [49]	90.90	103.73	0.72(7)	0.63(6)
	-18.053	C	62	77(9) [49]	89.78	101.10	0.86(10)	0.76(9)
	-18.045	Be	75	81(7) [50]	81.99	90.94	0.99(9)	0.89(8)
	-18.094	C	83	65(5) [52]	86.75	94.87	0.75(6)	0.69(5)
Average	-18.051						0.80(4)	0.71(3)
($^{14}\text{C}, ^{13}\text{C}$)	-10.807	C	67	65(4) [49]	133.284	148.61	0.49(3)	0.44(3)
	-10.800	C	83	67(14) [37]	130.74	142.66	0.51(13)	0.47(12)
	-10.767	C	235	80(7) [55]	110.92	121.39	0.72(6)	0.66(6)
Average	-10.793						0.53(3)	0.48(2)
($^{12}\text{C}, ^{11}\text{C}$)	3.259	C	95	53(22) [56]	102.21	111.06	0.52(22)	0.48(20)
	3.266	C	240	60.51(11.08) [57]	94.12	104.37	0.64(12)	0.58(11)
	3.265	C	250	56.0(41) [58]	93.73	104.31	0.60(4)	0.54(4)
Average	3.263						0.60(4)	0.54(4)
($^{10}\text{C}, ^9\text{C}$)	17.277	Be	120	23.4(11) [59]	47.40	51.65	0.49(2)	0.45(2)
	17.277	C	120	27.4(13) [59]	49.72	54.36	0.55(3)	0.50(2)
Average	17.277						0.52(2)	0.48(2)
($^9\text{C}, ^8\text{B}$)	-12.925	Be	67	48.6(73) [60]	62.77	66.67	0.77(12)	0.73(11)
	-12.925	Be	100	56(3) [61]	58.77	59.72	0.95(5)	0.94(5)
Average	-12.925						0.92(5)	0.90(5)
($^{12}\text{C}, ^{11}\text{B}$)	-2.237	C	230	63.9(66) [62]	103.75	105.33	0.62(6)	0.61(6)
	-2.237	C	250	65.6(26) [58]	102.93	105.36	0.64(3)	0.62(2)
Average	-2.237						0.63(2)	0.62(2)
($^{13}\text{C}, ^{12}\text{B}$)	13.523	C	234	39.5(60) [62]	79.69	81.55	0.43(5)	0.40(4)
($^{14}\text{C}, ^{13}\text{B}$)	12.830	C	235	41.3(27) [62]	78.65	81.43	0.53(3)	0.51(3)
($^{16}\text{C}, ^{15}\text{B}$)	18.303	Be	75	18(2) [50]	60.23	62.50	0.30(3)	0.29(3)
	18.303	Be	239	16(2) [63]	56.86	58.45	0.28(4)	0.27(3)
	18.303	C	239	18(2) [62]	54.57	55.87	0.33(4)	0.32(4)
Average	18.303						0.30(2)	0.28(2)
($^{15}\text{C}, ^{14}\text{B}$)	20.134	C	237	28.4(28) [62]	55.36	57.58	0.51(5)	0.49(5)

507 nucleon removal cross sections by using the NTG model and
 508 OLA. The case studied is the ${}^9\text{Be}({}^{19}\text{C}, {}^{18}\text{C})\text{X}$ reaction within
 509 the incident energy range from 64 to 400 MeV/nucleon. It is
 510 found that the σ_{-1n} values predicted with the NTG model are
 511 larger than those predicted with the OLA within the whole
 512 energy range. The difference is found to be larger at lower
 513 incident energies. It will also be larger when the separation
 514 energy of the nucleon is larger, which correspond to a smaller
 515 root-mean-square radius of the single-particle wave function.

516 Finally, we study how much the reduction factors of the
 517 single particle strengths obtained from single-nucleon re-
 518 moval reactions change when the NTG model is used instead
 519 of the OLA. The cases studied are one-nucleon removal reac-
 520 tions induced by ${}^{9-20}\text{C}$ isotopes on carbon and ${}^9\text{Be}$ targets.
 521 On average, the reduction factors obtained with the NTG
 522 model are found to be less than those with the OLA by 7.8%.
 523 We also found that the averaged differences in σ_{-1n} are larger

524 than those in σ_{-1p} , which are 10.6% and 4.2%, respectively.
 525 However, the linear dependence on the neutron-proton asym-
 526 metry of the reduction factors persists. Thus, the question of
 527 why the reduction factors of the single particle strengths from
 528 single-nucleon removal reaction measurements depend differ-
 529 ently on ΔS with respect to other types of reactions remains
 530 open even when the multiple scattering effect is included in
 531 the Glauber model analysis with the NTG model.

ACKNOWLEDGMENTS

532 This work was financially supported by the National Key
 533 R&D Program of China (Grant No. 2023YFA1606702)
 534 and the National Natural Science Foundation of China (Nos.
 535 U2067205 and 12205098). We thank Profs. J.A. Tostevin and
 536 W. Horiuchi for their helps during this work.

538 [1] N. K. Glendenning, in *Direct Nuclear Reactions*, (WORLD 539 SCIENTIFIC, 2004)

540 [2] B. P. Kay, J. P. Schiffer, S. J. Freeman, Quenching of cross 541 sections in nucleon transfer reactions, *Phys. Rev. Lett.*, **111**: 542 042502 (2013). [DOI:10.1103/PhysRevLett.111.042502](https://doi.org/10.1103/PhysRevLett.111.042502)

543 [3] B. P. Kay, T. L. Tang, I. A. Tolstukhin, *et al.*, Quenching of 544 single-particle strength in $a = 15$ nuclei, *Phys. Rev. Lett.*, **129**: 545 152501 (2022). [DOI:10.1103/PhysRevLett.129.152501](https://doi.org/10.1103/PhysRevLett.129.152501)

546 [4] V. R. Pharippe, I. Sick, P. K. A. d. Huberts, Independent parti- 547 cle motion correlations in fermion systems, *Rev. Mod. Phys.*, **69**: 548 981–991 (1997). [DOI:10.1103/RevModPhys.69.981](https://doi.org/10.1103/RevModPhys.69.981)

549 [5] W. Dickhoff C. Barbieri, Self-consistent green's function 550 method for nuclei nuclear matter, *Progress in Particle Nuclear 551 Physics*, **52**, 377–496 (2004). [DOI:10.1016/j.ppnp.2004.02.038](https://doi.org/10.1016/j.ppnp.2004.02.038)

552 [6] Y.P. Xu, D.Y. Pang, X.Y. Yun, *et al.*, Proton–neutron asym- 553 metry independence of reduced single-particle strengths de- 554 rived from (p, d)reactions , *Phys. Lett. B*, **790**: 308 2019. 555 [DOI:10.1016/j.physletb.2019.01.034](https://doi.org/10.1016/j.physletb.2019.01.034)

556 [7] W. Liu, J.L. Lou, Y.L. Ye and D.Y. Pang, Experimental study 557 of intruder components in light neutron-rich nuclei via single- 558 nucleon transfer reaction, *Nucl. Sci. Tech.*, **31**: 20 2020. 559 [DOI:10.1007/s41365-020-0731-y](https://doi.org/10.1007/s41365-020-0731-y)

560 [8] S.L. Chen, Z.X. Liu, Z. Zhang *et al.*, Systematic investiga- 561 tion of nucleon optical model potentials in (p, d) transfer re- 562 actions, *Chin. Phys. C*, **48**: 074104 2024. [DOI:10.1088/1674-1137/ad4269](https://doi.org/10.1088/1674-1137/ad4269)

563 [9] L. Atar, S. Paschalis, C. Barbieri,*et al.*, Quasifree ($p, 2p$) reac- 564 tions on oxygen isotopes: Observation of isospin independence 565 of the reduced single-particle strength, *Phys. Rev. Lett.*, **120**: 566 052501 (2018). [DOI:10.1103/PhysRevLett.120.052501](https://doi.org/10.1103/PhysRevLett.120.052501)

567 [10] F. Flavigny, N. Keeley, A. Gillibert, A. Obertelli, Single- 568 particle strength from nucleon transfer in oxygen isotopes: 569 Sensitivity to model parameters, *Phys. Rev. C*, **97**: 034601 570 (2018). [DOI:10.1103/PhysRevC.97.034601](https://doi.org/10.1103/PhysRevC.97.034601)

571 [11] J. A. Tostevin A. Gade, Systematics of intermediate-energy 572 single-nucleon removal cross sections, *Phys. Rev. C*, **90**: 573 057602 (2014). [DOI:10.1103/PhysRevC.90.057602](https://doi.org/10.1103/PhysRevC.90.057602)

574 [12] J. A. Tostevin A. Gade, Updated systematics of intermediate- 575 energy single-nucleon removal cross sections, *Phys. Rev. C*, **103**: 576 054610 (2021). [DOI:10.1103/PhysRevC.103.054610](https://doi.org/10.1103/PhysRevC.103.054610)

577 [13] P. Hansen J. Tostevin, Direct reactions with exotic nuclei, *Annual Review of Nuclear Particle Science*, **53** :219–261 (2003). [DOI:10.1146/annurev.nucl.53.041002.110406](https://doi.org/10.1146/annurev.nucl.53.041002.110406)

578 [14] T. Pohl, Y. L. Sun, A. Obertelli, *et al.*, Multiple 579 mechanisms in proton-induced nucleon removal at \sim 580 100 MeV/Nucleon, *Phys. Rev. Lett.*, **130**: 172501 (2023). [DOI:10.1103/PhysRevLett.130.172501](https://doi.org/10.1103/PhysRevLett.130.172501)

581 [15] E. C. Simpson J. A. Tostevin, One- two-neutron removal from 582 the neutron-rich carbon isotopes, *Phys. Rev. C*, **79**: 024616 583 (2009). [DOI:10.1103/PhysRevC.79.024616](https://doi.org/10.1103/PhysRevC.79.024616)

584 [16] C. Bertulani, Core destruction in knockout reac- 585 tions, *Physics Letters B*, **846**: 138250 (2023). [DOI:10.1016/j.physletb.2023.138250](https://doi.org/10.1016/j.physletb.2023.138250)

585 [17] M.Q. Ding, D.Q. Fang and Y.G. Ma, Neutron skin and its ef- 586 fects in heavy-ion collisions, *Nucl. Sci. Tech.*, **35**: 211 2024. [DOI:10.1007/s41365-024-01584-1](https://doi.org/10.1007/s41365-024-01584-1)

587 [18] Y.H. Wang, D.Y. Pang, W.D. Chen, *et al.*, Nuclear radii 588 from total reaction cross section measurements at interme- 589 diate energies with complex turning point corrections to 590 the eikonal model, *Phys. Rev. C*, **109**: 014621 (2024). [DOI:10.1103/PhysRevC.109.014621](https://doi.org/10.1103/PhysRevC.109.014621)

589 [19] J.F. Wang, H.J. Xu and F.Q. Wang, Impact of initial fluctuations 590 and nuclear deformations in isobar collisions, *Nucl. Sci. Tech.*, **35**: 108 2024. [DOI:10.1007/s41365-024-01480-8](https://doi.org/10.1007/s41365-024-01480-8)

591 [20] Y. Suzuki, K. Yabana, R. G. Lovas, K. Varga, in *Structure 592 Reactions of Light Exotic Nuclei*, (Taylor & Francis, 2003).

592 [21] B. Abu-Ibrahim Y. Suzuki, Scatterings of complex nuclei 593 in the glauber model, *Phys. Rev. C*, **62**: 034608 (2000). [DOI:10.1103/PhysRevC.62.034608](https://doi.org/10.1103/PhysRevC.62.034608)

594 [22] B. Abu-Ibrahim Y. Suzuki, Utility of nucleon-target profile 595 function in cross section calculations, *Phys. Rev. C*, **61**: 051601 596 (2000). [DOI:10.1103/PhysRevC.61.051601](https://doi.org/10.1103/PhysRevC.61.051601)

597 [23] W. Horiuchi1, Y. Suzuki, B. Abu-Ibrahim *et al.*, Systematic 598 analysis of reaction cross sections of carbon isotopes, *Phys. 599 Rev. C*, **76**: 044607 (2007). [DOI:10.1103/PhysRevC.75.044607](https://doi.org/10.1103/PhysRevC.75.044607)

600 [24] R. J. Glauber, in *Lectures on Theoretical Physics*, (Interscience, 601 New York, 1959)

601 [25] S. Hatakeyama, S. Ebata, W. Horiuchi, and M. Kimura, 602 Multiple-scattering effects in proton- and alpha-nucleus reac- 603 tions with Glauber theory, *J. Phys. Conf. Ser.*, **569**: 012050 604 (2014).[doi:10.1088/1742-6596/569/1/012050](https://doi.org/10.1088/1742-6596/569/1/012050)

619 [26] L. Ray, Proton-nucleus total cross sections in the intermediate energy range, Phys. Rev. C, **20**:1857–1872, (1979).
 620 DOI:[10.1103/PhysRevC.20.1857](https://doi.org/10.1103/PhysRevC.20.1857)

621 [27] C. Werneth, X. Xu, R. Norman, W. Ford, K. Maung, Validation of elastic cross section models for space radiation applications, Nuclear Instruments Methods in Physics Research Section B: Beam Interactions with Materials Atoms, **392**,74–93 (2017).
 622 DOI:[10.1016/j.nimb.2016.12.009](https://doi.org/10.1016/j.nimb.2016.12.009)

623 [28] R. L. Workman *et.al.*, Review of particle physics, PTEP, **2022**: 083C01 (2022). DOI:[10.1093/ptep/ptac097](https://doi.org/10.1093/ptep/ptac097)

624 [29] J. A. Tostevin, Cross sections of removal reactions populating weakly-bound residual nuclei , (2022).
 625 DOI:[10.48550/arXiv.2203.06058](https://doi.org/10.48550/arXiv.2203.06058)

626 [30] T. Nagahisa W. Horiuchi, Examination of the ^{22}C radius determination with interaction cross sections, Phys. Rev. C, **97**: 054614 (2018). DOI:[10.1103/PhysRevC.97.054614](https://doi.org/10.1103/PhysRevC.97.054614)

627 [31] C. Bertulani A. Gade, Momdis: a glauber model computer code for knockout reactions, Computer Physics Communications, **175**,372–380 (2006). DOI:[10.1016/j.cpc.2006.04.006](https://doi.org/10.1016/j.cpc.2006.04.006)

628 [32] J.A. Tostevin, M.H. Lopes, and R.C. Johnson, Elastic scattering and deuteron-induced transfer reactions, Nucl. Phys. A, **465**: 83-122 (1984). DOI:[10.1016/0375-9474\(87\)90300-9](https://doi.org/10.1016/0375-9474(87)90300-9)

629 [33] M. Takechi, M. Fukuda, M. Mihara, *et al.*, Reaction cross sections at intermediate energies and Fermi-motion effect, Phys. Rev. C, **79**: 061601(R) (2009).
 630 DOI:[10.1103/PhysRevC.79.061601](https://doi.org/10.1103/PhysRevC.79.061601)

631 [34] J. Hostachy, M. Buenerd, J. Chauvin,*et.al.*, Elastic inelastic scattering of ^{12}C ions at intermediate energies, Nucl. Phys. A, **490**,441–470 (1988). DOI:[10.1016/0375-9474\(88\)90514-3](https://doi.org/10.1016/0375-9474(88)90514-3)

632 [35] M. Buenerd, A. Lounis, J. Chauvin, D. Lebrun: Martin, G. Duhamel, J. Gondr, P. De Saintignon, Elastic inelastic scattering of carbon ions at intermediate energies, Nucl. Phys. A, **424**: 313–334 (1984). DOI:[10.1016/0375-9474\(84\)90186-6](https://doi.org/10.1016/0375-9474(84)90186-6)

633 [36] D.T. Khoa, α -nucleus optical potential in the double-folding model, Phys. Rev. C, **63**: 034007 (2018). DOI:[10.1103/PhysRevC.63.034007](https://doi.org/10.1103/PhysRevC.63.034007)

634 [37] D. Q. Fang, T. Yamaguchi, T. Zheng, *et al.*, One-neutron halo structure in ^{15}C , Phys. Rev. C, **69**: 034613 (2004). DOI:[10.1103/PhysRevC.69.034613](https://doi.org/10.1103/PhysRevC.69.034613)

635 [38] S. Kox, A. Gamp, C. Perrin, *et al.*, Trends of total reaction cross sections for heavy ion collisions in the intermediate energy range, Phys. Rev. C, **35**,1678–1691 (1987). DOI:[10.1103/PhysRevC.35.1678](https://doi.org/10.1103/PhysRevC.35.1678)

636 [39] J. Jaros, A. Wagner, L. erson,*et al.*, Nucleus-nucleus total cross sections for light nuclei at 1.55–2.89 gev/c per nucleon, Phys. Rev. C, **18**,2273–2292 (1978). DOI:[10.1103/PhysRevC.18.2273](https://doi.org/10.1103/PhysRevC.18.2273)

637 [40] T. Zheng, T. Yamaguchi, A. Ozawa, *et al.*, Study of halo structure of ^{16}C from reaction cross section measurement, Nuclear Physics A, **709**, 103–118 (2002). DOI:[10.1016/S0375-9474\(02\)01043-6](https://doi.org/10.1016/S0375-9474(02)01043-6)

638 [41] H. Zhang, W. Shen, Z. Ren, *et al.*, Measurement of reaction cross section for proton-rich nuclei ($a < 30$) at intermediate energies, Nuclear Physics A, **707**, 303–324 (2002). DOI:[10.1016/S0375-9474\(02\)01007-2](https://doi.org/10.1016/S0375-9474(02)01007-2)

639 [42] C. Perrin, S. Kox, N. Longequeue, *et al.*, Direct measurement of the $^{12}\text{C} + ^{12}\text{C}$ reaction cross section between 10–83 mev/nucleon, Phys. Rev. Lett., **49**, 1905–1909, (1982). DOI:[10.1103/PhysRevLett.49.1905](https://doi.org/10.1103/PhysRevLett.49.1905)

640 [43] M. Takechi, M. Fukuda, M. Mihara, *et al.*, Reaction cross-sections for stable nuclei nucleon density distribution of proton drip-line nucleus ^{8}B , The European Physical Journal A, **25**, 217–219, (2005). DOI:[10.1140/epjad/i2005-06-078-0](https://doi.org/10.1140/epjad/i2005-06-078-0)

641 [44] L. Ponnath, T. Aumann, C. Bertulani, *et al.*, Measurement of nuclear interaction cross sections towards neutron-skin thickness determination, Physics Letters B, **855**:138780 (2024). DOI:[10.1016/j.physletb.2024.138780](https://doi.org/10.1016/j.physletb.2024.138780)

642 [45] K. Hencken, G. Bertsch, H. Esbensen, Breakup reactions of the halo nuclei ^{11}Be ^{8}B , Phys. Rev. C, **54**, 3043–3050 (1996). DOI:[10.1103/PhysRevC.54.3043](https://doi.org/10.1103/PhysRevC.54.3043)

643 [46] A.E.L. Dieperink and T. de Forest, Phys. Rev. C 10, 543 (1974). DOI: <https://doi.org/10.1103/PhysRevC.10.543>

644 [47] Y.-P. Xu, D.-Y. Pang, C.-X. Yuan, X.-Y. Yun, Quenching of single-particle strengths of carbon isotopes 9-12,14-20c with knockout reactions for incident energies 43-2100 mev/nucleon *, Chinese Physics C, **46**: 064102 (2022). DOI:[10.1088/1674-1137/ac5236](https://doi.org/10.1088/1674-1137/ac5236)

645 [48] W. L. Hai, D. Y. Pang, X. B. Wang, *et al.*, Determining the radii of single particle potentials with skyrme hartree fock calculations, Phys. Rev. C, **110**:044613 (2024). DOI:[10.1103/PhysRevC.110.044613](https://doi.org/10.1103/PhysRevC.110.044613)

646 [49] E. Sauvan, F. Carstoiu, N. A. Orr,*et al.*, One-neutron removal reactions on light neutron-rich nuclei, Phys. Rev. C, **69**: 044603 (2004). DOI:[10.1103/PhysRevC.69.044603](https://doi.org/10.1103/PhysRevC.69.044603)

647 [50] F. Flavigny, A. Obertelli, A. Bonaccorso, *et al.*, Nonsudden limits of heavy-ion induced knockout reactions, Phys. Rev. Lett., **108**: 252501 (2012). DOI:[10.1103/PhysRevLett.108.252501](https://doi.org/10.1103/PhysRevLett.108.252501)

648 [51] N. Kobayashi, T. Nakamura, J. A. Tostevin,*et al.*, One-two-neutron removal reactions from the most neutron-rich carbon isotopes, Phys. Rev. C, **86**: 054604 (2012). DOI:[10.1103/PhysRevC.86.054604](https://doi.org/10.1103/PhysRevC.86.054604)

649 [52] V. Maddalena, T. Aumann, D. Bazin, *et al.*, Single-neutron knockout reactions: Application to the spectroscopy of $^{16,17,19}\text{C}$, Phys. Rev. C, **63**: 024613 (2001). DOI:[10.1103/PhysRevC.63.024613](https://doi.org/10.1103/PhysRevC.63.024613)

650 [53] J. R. Terry, D. Bazin, B. A. Brown,*et al.*, Absolute spectroscopic factors from neutron knockout on the halo nucleus ^{15}C , Phys. Rev. C, **69**: 054306 (2004). DOI:[10.1103/PhysRevC.69.054306](https://doi.org/10.1103/PhysRevC.69.054306)

651 [54] C. Wu, Y. Yamaguchi, A. Ozawa, I. Tanihata, D. Jiang, H. Hua, T. Zheng, Z. Li, Y. Ye, Neutron removal reactions of ^{17}C , Journal of Physics G: Nuclear Particle Physics, **31**: 39 (2004). DOI:[10.1088/0954-3899/31/1/004](https://doi.org/10.1088/0954-3899/31/1/004)

652 [55] Y. Z. Sun, S. T. Wang, Z. Y. Sun, *et al.*, Single-neutron removal from $^{14,15,16}\text{C}$ near 240 mev/nucleon, Phys. Rev. C, **104**: 014310 (2021). DOI:[10.1103/physrevc.104.014310](https://doi.org/10.1103/physrevc.104.014310)

653 [56] J. Dudouet, D. Juliani, M. Labalme, *et al.*, Double-differential fragmentation cross-section measurements of 95 mev/nucleon ^{12}C beams on thin targets for hadron therapy, Phys. Rev. C, **88**: 024606 (2013). DOI:[10.1103/PhysRevC.88.024606](https://doi.org/10.1103/PhysRevC.88.024606)

654 [57] Y. SUN, Y. ZHAO, S. JIN, *et al.*, Data analysis framework for radioactive ion beam experiments at the external target facility of hirfl-csr, Nuclear Physics Review, **37**: 742 (2020). DOI:[10.11804/NuclPhysRev.37.2019CNPC27](https://doi.org/10.11804/NuclPhysRev.37.2019CNPC27)

655 [58] B. A. Brown: G. Hansen, B. M. Sherrill, J. A. Tostevin, Absolute spectroscopic factors from nuclear knockout reactions, Phys. Rev. C, **65**: 061601 (2002). DOI:[10.1103/PhysRevC.65.061601](https://doi.org/10.1103/PhysRevC.65.061601)

656 [59] G. F. Grinyer, D. Bazin, A. Gade, *et al.*, Systematic study of p -shell nuclei via single-nucleon knockout reactions, Phys. Rev. C, **86**: 024315 2012. DOI:[10.1103/PhysRevC.86.024315](https://doi.org/10.1103/PhysRevC.86.024315)

657 [60] R. J. Charity, L. G. Sobotka, J. A. Tostevin, Single-nucleon knockout cross sections for reactions producing resonance states at or beyond the drip line, Phys. Rev. C, **102**: 044614 (2020). DOI:[10.1103/PhysRevC.102.044614](https://doi.org/10.1103/PhysRevC.102.044614)

745 [61] D. Bazin, R. J. Charity, R. T. de Souza,*et al.*, Mechanisms 755 [64] F. Flavigny, A. Gillibert, L. Nalpas, *et al.*, Limited
746 in knockout reactions, Phys. Rev. Lett., **102**: 232501 (2009). 756 asymmetry dependence of correlations from single nu-
747 DOI:[10.1103/PhysRevLett.102.232501](https://doi.org/10.1103/PhysRevLett.102.232501) 757 cleon transfer, Phys. Rev. Lett., **110**: 122503 (2013).
758 DOI:[10.1103/PhysRevLett.110.122503](https://doi.org/10.1103/PhysRevLett.110.122503)

748 [62] Y. Z. Sun, S. T. Wang, Z. Y. Sun, *et al.*, One-proton removal 759 [65] M. Gómez-Ramos A. Moro, Binding-energy independence of
749 from neutron-rich carbon isotopes in $^{12-16}\text{C}$ beams near 240 760 reduced spectroscopic strengths derived from (p,2p) (p,pn) re-
750 mev/nucleon beam energy, Phys. Rev. C, **110**: 014603 (2024). 761 actions with nitrogen oxygen isotopes, Physics Letters B, **785**,
751 DOI:[10.1103/PhysRevC.110.014603](https://doi.org/10.1103/PhysRevC.110.014603) 762 511–516 (2018). DOI:[10.1016/j.physletb.2018.08.058](https://doi.org/10.1016/j.physletb.2018.08.058)

752 [63] Y. X. Zhao, Y. Z. Sun, S. T. Wang,*et al.*, One-proton knock- 763

753 out from ^{16}C at around 240 mev/nucleon, Phys. Rev. C, **100**: 764 044609 (2019). DOI:[10.1103/PhysRevC.100.044609](https://doi.org/10.1103/PhysRevC.100.044609)